Journal of Solid State Chemistry 183 (2010) 1007–1012

Contents lists available at ScienceDirect

Journal of Solid State Chemistry

journal homepage: www.elsevier.com/locate/jssc

Degree of order and redox balance in *B*-site ordered double-perovskite oxides, $Sr_2MMoO_{6-\delta}$ (M=Mg, Mn, Fe, Co, Ni, Zn)

S. Vasala [a], M. Lehtimäki [a,b], Y.H. Huang [b,c], H. Yamauchi [a], J.B. Goodenough [b], M. Karppinen [a,*]

[a] Laboratory of Inorganic Chemistry, Department of Chemistry, Aalto University School of Science and Technology, P.O. Box 16100, FI-00076 AALTO, Finland
[b] Texas Materials Institute, The University of Texas at Austin, Austin, TX 78712, USA
[c] School of Materials Science and Engineering, Huazhong University of Science and Technology, Hubei 430074, China

ARTICLE INFO

Article history:
Received 5 January 2010
Received in revised form
28 February 2010
Accepted 1 March 2010
Available online 6 March 2010

Keywords:
Double perovskite
Cation ordering
Oxygen nonstoichiometry
Redox chemistry
Mixed valency

ABSTRACT

We have investigated a series of double-perovskite oxides $Sr_2MMoO_{6-\delta}$ (M=Mg, Mn, Fe, Co, Ni, Zn) for redox stability, oxygen content and crystal structure. Phases with M=Co, Ni and Zn were found to be oxygen-stoichiometric and stable under oxidizing conditions, whereas those with M=Mn and Fe were oxygen-deficient and stable under reducing conditions. The M=Mg phase is stable both under reducing and oxidizing conditions, showing variable oxygen contents within $0.00 \le \delta \le 0.04$ depending on the annealing conditions. Structural data indicate somewhat depressed values for the degree of M/Mo cation order and also evidence of electron transfer from M^{II} to Mo^{VI} for M=Mn, Fe and Co.

1. Introduction

The structure of the *B*-site ordered double-perovskite oxides, $A_2B'B''O_{6-\delta}$, is derived from that of the simple perovskites, ABO_3, by having the *B*-cation site alternately occupied by two different cation species, B' and B''. In the former structure – in an ideal case – the B' cation has only B'' cations as nearest cation neighbors and *vice versa*, and accordingly the unit cell of *B*-site ordered double perovskite is 8 ($=2\times2\times2$) times larger than the primitive cubic cell of single perovskites. Such a cation ordering is not always complete, and rather common is that some degree of mixing between the B' and B'' cations is seen [1–3]. The smaller the differences between the sizes and charges of the two *B*-site cations, the lower is the equilibrium degree of order at the *B* site [1–3]. Thermodynamics tells us that samples with the highest degree of order are obtained using low synthesis temperatures. However, at low temperatures cation diffusion becomes slow and the degree of order is rather kinetically controlled. Thus, to obtain highly ordered double-perovskite samples in practice, relatively long synthesis periods at moderate temperatures are required [1–3].

A number of *B*-site ordered double-perovskite materials with different cation compositions have been studied since 1960s [4–6], and in particular for the last decade owing to the discovery of room-temperature half-metallicity and a large intergrain tunneling magnetoresistance effect in $Sr_2FeMoO_{6-\delta}$ in 1998 [7,8]. More recently it was found that another very similar *B*-site ordered double perovskite, i.e. $Sr_2MgMoO_{6-\delta}$, is a promising anode material for solid oxide fuel cells (SOFCs) [9]. A necessary requirement for a material to perform well as an SOFC anode is that it is simultaneously a good electron and oxide-ion conductor in a reducing atmosphere. In $Sr_2MgMoO_{6-\delta}$ this condition is achieved by the presence of oxygen vacancies [10], which are critical not only for fast oxide-ion diffusion but also for $Mo^{V/VI}$ mixed valency and charge-carrier doping [9]. The $Sr_2FeMoO_{6-\delta}$ compound, on the other hand, is essentially stoichiometric, i.e. $\delta \approx 0$ [11,12], and hence "self-doped" [8]. Band-structure calculations have revealed strong mixing of the itinerant *d* electron from formally pentavalent Mo ($4d^1$; t_{2g}^1; $S=1/2$) and the minority spin t_{2g} band of formally trivalent, high-spin Fe ($3d^5$; $t_{2g}^3e_g^2$; $S=5/2$) in Sr_2FeMoO_6 [7,13–16], and accordingly mixed-valence states of II/III and V/VI for Fe and Mo, respectively. In fact, the *B*-cation valence states in $A_2B'B''O_6$ double-perovskite oxides has been a topic of discussion since the 1970s [17,18]. Experimental evidence for the iron mixed valency in $Sr_2FeMoO_{6-\delta}$ has been obtained by two spectroscopy probes, Mössbauer [19] and XANES [20], and for the Mo mixed valency by means of the NMR technique [21]. Moreover, neutron diffraction [22–25] and X-ray magnetic circular dichroism [26] data have revealed reduced magnetic moment values at both the Fe and the Mo sites from the values expected for high-spin Fe^{III} and Mo^{V}.

Here we investigate a series of $Sr_2MMoO_{6-\delta}$ compounds with M=Mg, Mn, Fe, Co, Ni and Zn for their crystal structure, redox stability and precise oxygen content in order to address

* Corresponding author. Fax: +358 9 462 373.
E-mail address: maarit.karppinen@tkk.fi (M. Karppinen).

0022-4596/$ - see front matter © 2010 Elsevier Inc. All rights reserved.
doi:10.1016/j.jssc.2010.03.004

systematically the questions concerning the cation (dis)order, oxygen (non)stoichiometry and valence mixing in *B*-site ordered double-perovskite oxides. The M=Mg and Zn compounds of the series represent cases in which no charge transfer between the two different *B*-cation species, i.e. *M* and Mo, is expected from basic chemistry considerations, whereas for the rest of the compounds the *B*′-site constituent, i.e. *M*, is a 3*d* transition metal and accordingly prone to transfer electrons to Mo-5*d* orbitals.

2. Experimental

Homogeneous precursors for the $Sr_2MMoO_{6-\delta}$-sample (M=Mg, Mn, Fe, Co, Ni, Zn) synthesis were prepared through a wet-chemical route in which stoichiometric amounts of starting-material powders, $SrCO_3$, MgO, $MnCO_3$, $FeC_2O_4\cdot 2H_2O$, Co $(CH_3COO)_2\cdot 4H_2O$, $Ni(CH_3COO)_2\cdot 4H_2O$, ZnO and $(NH_4)_6Mo_7O_{24}\cdot 3.6H_2O$, are dissolved in an aqueous HNO_3 solution. *Prior* to this, contents of crystal-lattice water were determined for the starting materials by thermogravimetric analysis. In addition, MgO powder was calcined in air at 850 °C to decompose any traces of the hydrates and carbonates. A separate ethylenediaminetetraacetic acid (EDTA) solution was prepared by dissolving EDTA in an aqueous NH_3 solution. The molar amount of EDTA in the solution was adjusted to be 1.5 times the total amount of metal cations. The EDTA solution was then slowly poured into the solution containing the metal cations, followed by the final adjustment of the pH value to 9–10 with NH_3/H_2O. This solution was then heated on a heating plate for chelation and to remove excess water. The resultant dry gel was burned to obtain a powder that was calcined in a box furnace at 900 °C in air for 12 h. Then the sample powder was thoroughly ground and pressed into pellets for sintering in 5% H_2/Ar at 1000 °C for M=Mg, Mn and Fe and in air at 1200 °C for M=Co, Ni and Zn. Typically one-time sintering of 24 h was enough, except for $Sr_2FeMoO_{6-\delta}$ for which a second-time grinding and sintering of 20 h was needed to achieve decent purity.

Phase purity and crystal-structure parameters of the samples were examined by X-ray powder diffraction (XRD; Philips MPD 1880) using Cu *K*α radiation. The XRD patterns were analyzed with the Rietveld refinement program FULLPROF [27] in triclinic space group $I-1$, as utilized by Bernuy-Lopez et al. [28] for $Sr_2MgMoO_{6-\delta}$. Even though some high symmetry space groups, e.g. $I4/mmm$, $I/4m$ and $P2_1/n$, had been employed for some of the $Sr_2MMoO_{6-\delta}$ compounds, the lower symmetry space group *I*–1 (which can be thought of as a different setting of the *P*–1 space group) was selected here for all the samples for easy comparison. The degree of *B*-site cation order was determined by refining the partial occupancy of *M* atoms at the Mo site and *vice versa*. In these refinements the overall occupancy at the octahedral Mo [2(*a*)] and *M* [2(*b*)] sites was fixed to unity together with the overall Mo and *M* compositions which were also fixed to the unity (such that the Mo and *M* atoms were only let to change places). The degree of order, *S*, was defined as $S=2(g_M-0.5)$ (where g_M is the occupancy of *M* cation at its right site) such that for $S=1$ the structure is perfectly ordered and for $S=0$ completely disordered.

The redox behaviors of the samples, i.e. the chemical stability and the changes in oxygen content under reduction/oxidation, were studied by thermogravimetric (TG) analyses (Perkin Elmer Pyris 1 TGA). The samples were studied either in air or in 5% H_2/Ar atmospheres depending on their preparation history, such that samples synthesized in 5% H_2/Ar were oxidized in air whereas those synthesized in air were reduced in 5% H_2/Ar. In the TG experiment, the sample was heated to 1000 °C at a rate of 2 °C/min and cooled back to room temperature at a rate of 2 °C/min.

The precise oxygen content, $6-\delta$, was determined for each sample employing a wet-chemical redox-analysis method with which the total amount of reduced (lower-valent) species of Mo and/or the transition metal *M* is determined with Fe^{III} as an oxidant and then back-oxidizing the resultant Fe^{II} species through coulometric titration [11,12,29]. Possible traces of Mn^{III}, Co^{III} and Ni^{III} in the sample are reduced by Fe^{II} to the +II valence state, as dictated by the standard reduction potentials of these species [30]. It should be noted that potentials required to oxidize any of these divalent cations (other than Fe^{II}) present in the titration cell solution are much higher than that for the oxidation of Fe^{II}. These cations do not therefore disturb the titration. For the analysis, an accurately weighted power specimen of 20–30 mg was dissolved in 200 ml of 3 M HCl containing an excess of Fe^{III} ions. The HCl solution was bubbled with N_2 *prior* to use to remove any dissolved oxygen, and the titration was performed under N_2 atmosphere. The electrochemical oxidation of Fe^{II} was performed with a constant current of 1 mA until the potential against an Ag/AgCl electrode reached 820 mV. The analysis was typically repeated three times, with the standard deviation of oxygen-deficiency value δ being ± 0.002–0.007, depending on the sample.

3. Results and discussion

Fig. 1 shows X-ray diffraction patterns for the $Sr_2MMoO_{6-\delta}$ samples after an initial calcination in air at 900 °C. Some of the samples (with M=Ni, Mg, Zn and Co) contain small amounts of the target double-perovskite phase already at this stage of synthesis, but other samples (with M=Fe, Mn) do not. In Fig. 1, also given are values of the Goldschmidt tolerance factor $[t=(r_A+r_O)/\sqrt{2}(r_B+r_O)]$, calculated for each sample composition from the ionic radius values, r_A, r_B and r_O, tabulated by Shannon [31,32]. The *t* value is commonly used as a measure for the stability of the perovskite structure (such that $t=1$ corresponds to ideal bond-length matching and highest stability). Here all the *t* values are less than unity. Interestingly, from Fig. 1 we may conclude that double-perovskite phase formation occurs already during the initial calcination step in air for $Sr_2MMoO_{6-\delta}$ samples with $t>0.97$.

Based on the aforementioned phase-formation information after calcination in air and also on the synthesis conditions previously reported for some of the $Sr_2MMoO_{6-\delta}$ compositions [3,9,33], the samples with M=Mg, Mn and Fe were sintered in 5% H_2/Ar at 1000 °C while those with M=Co, Ni and Zn were sintered in air at 1200 °C. Note that $Sr_2MgMoO_{6-\delta}$ can be synthesized both

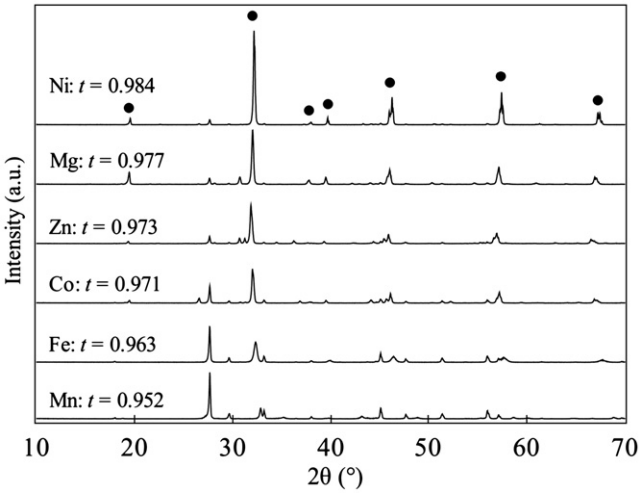

Fig. 1. X-ray diffraction patterns for the $Sr_2MMoO_{6-\delta}$ samples (M=Mg, Mn, Fe, Co, Ni, Zn) after the initial calcination in air at 900 °C for 12 h. Peaks due to the emerging double-perovskite phase are marked with filled circles (●). Note that the patterns are arranged in the order of decreasing value of tolerance factor (*t*).

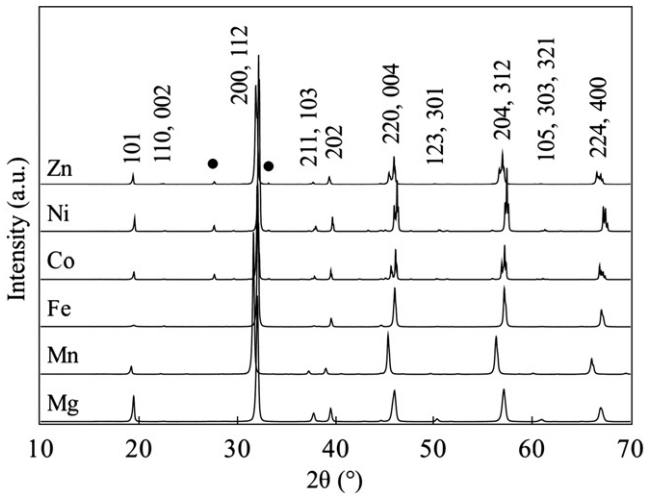

Fig. 2. X-ray diffraction patterns for the as-synthesized $Sr_2MMoO_{6-\delta}$ (M=Mg, Mn, Fe, Co, Ni, Zn) double-perovskite samples. The *hkl* indices are for the space group $I-1$. Peaks due to the $SrMoO_4$ impurity phase are marked with filled circles (●).

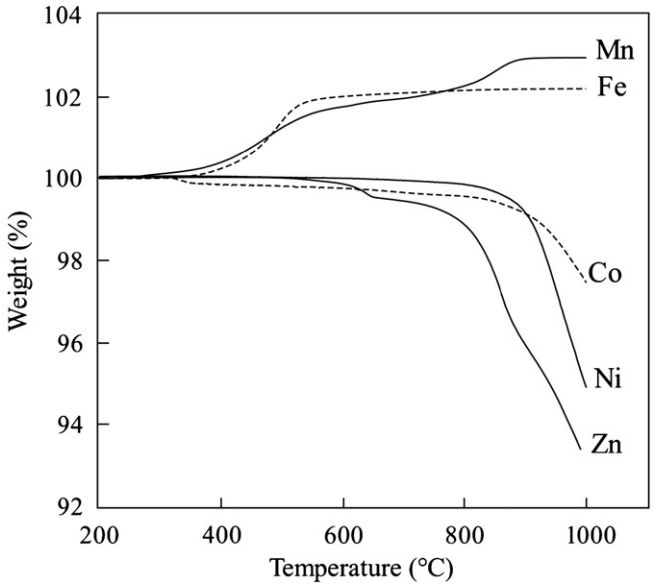

Fig. 3. TG curves for the oxidation of the as-synthesized $Sr_2MnMoO_{6-\delta}$ and $Sr_2FeMoO_{6-\delta}$ samples in air and for the reduction of the as-synthesized $Sr_2CoMoO_{6-\delta}$, $Sr_2NiMoO_{6-\delta}$ and $Sr_2ZnMoO_{6-\delta}$ samples in 5% H_2/Ar.

in air and in 5% H_2/Ar, but in the latter case at a lower temperature [34]. Fig. 2 shows X-ray diffraction patterns for the final $Sr_2MMoO_{6-\delta}$ samples. The samples were found to be nearly phase-pure, although small amounts of $SrMoO_4$ (of the order of 2% according to Rietveld refinement) were detected in all the samples sintered in air. Moreover, some weak extra reflections were seen for $Sr_2CoMoO_{6-\delta}$, but unfortunately could not be reliably identified.

The colors of the samples are worth noting: $Sr_2MnMoO_{6-\delta}$, $Sr_2FeMoO_{6-\delta}$ and $Sr_2CoMoO_{6-\delta}$ are black, $Sr_2NiMoO_{6-\delta}$ rusty orange and $Sr_2ZnMoO_{6-\delta}$ slightly yellowish. The color of $Sr_2MgMoO_{6-\delta}$ apparently depends on the degree of reduction. When sintered in air, $Sr_2MgMoO_{6-\delta}$ was almost white, with a slight yellowish or greenish tint. When sintered under reducing conditions or reduced afterwards, it turned into grayish blue and the color intensity increased with increasing degree of reduction.

The as-synthesized samples were studied through TG annealing experiments for their redox stabilities. The samples with M=Co, Ni and Zn (initially sintered in air) were reduced in 5% H_2/Ar, and the samples with M=Mn and Fe (sintered in 5% H_2/Ar) were oxidized in air. Fig. 3 shows the corresponding TG curves. In the case of the former air-sintered samples with M=Co, Ni and Zn, small mass drops are seen at 350 °C (Co) and 600 °C (Zn), but the full-scale reduction starts at 800–900 °C, after which the samples were found to have been decomposed (by XRD; data not shown here). Here we note that Huang et al. [33] noticed similar decomposition of the M=Co or Ni phases above 800 °C, whereas Wei et al. [35] reported successful synthesis of $Sr_2NiMoO_{6-\delta}$ in 5% H_2/Ar at 1100 °C, which disagrees with the present observation. We found no explanation for this disagreement, but in out tests the M=Co or Ni phases could not be synthesized under reducing conditions. As for the M=Mn and Fe samples, the weight gain starts below 400 °C upon annealing in air and both samples decompose already during this low-temperature oxidation step. These results are consistent with a progressive lowering of the energy of the M-4*s* band with increasing atomic number of the 3*d*-block cations [36]. The TG data for the $Sr_2MgMoO_{6-\delta}$ sample are displayed in Fig. 4: shown are TG curves for subsequent oxidative (in air) and reductive (in 5% H_2/Ar) annealing cycles. Unlike the samples containing 3*d* transition metals, $Sr_2MgMoO_{6-\delta}$ withstands the oxidation–reduction cycling without degradation. As is seen in Fig. 4, during the oxidation–reduction annealings the overall mass changes of the sample are rather reversible.

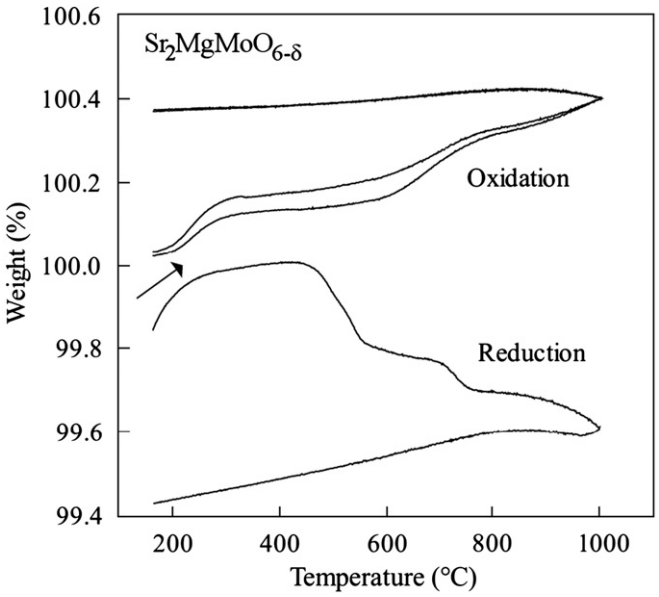

Fig. 4. TG curves for consecutive oxidation (air) – reduction (5% H_2/Ar) – oxidation (air) cycling of the $Sr_2MgMoO_{6-\delta}$ sample synthesized in 5% H_2/Ar.

Coulometric titration was used to determine precise oxygen contents of the as-synthesized $Sr_2MMoO_{6-\delta}$ samples. Results are presented in Table 1. They show that the samples with M=Ni and Zn (sintered in air) are oxygen-stoichiometric, i.e. δ=0.000(2). Titration results for $Sr_2CoMoO_{6-\delta}$ suggest at first glance that it is over-oxidized, i.e. $\delta=-0.011(2)$. However, the negative δ value may equally well originate from tiny amounts of impurities containing trivalent cobalt. As noted before, some unidentified diffraction peaks were seen in the XRD patterns of $Sr_2CoMoO_{6-\delta}$. These reflections were very weak, but some of them matched those of Co_3O_4, which could explain the titration results. The ratio of Co^{III}/Co was estimated by titration to be ~2%, which is of the same order as that of the $SrMoO_4$ impurity. The samples with M=Mg, Mn and Fe (sintered in 5% H_2/Ar) are all found to be oxygen nonstoichiometric with $\delta > 0$ (see Table 1). The δ value of

0.040(2) for M=Mg agrees well with one (~0.05) previously determined for another $Sr_2MgMoO_{6-\delta}$ sample similarly synthesized [10]. In the case of $Sr_2FeMoO_{6-\delta}$, the previously reported δ values (~0.03) are for samples synthesized by a somewhat different method [11,12]. Nevertheless, a rather close value of δ=0.041(7) was obtained for the present $Sr_2FeMoO_{6-\delta}$ sample. Finally, we confirmed the reversibility of the δ value for $Sr_2MgMoO_{6-\delta}$ by coulometric titration upon subsequent oxidative (in air) and reductive (in 5% H_2/Ar) annealing cycles. The $Sr_2MgMoO_{6-\delta}$ sample annealed in air was found to be oxygen-stoichiometric with δ=0.000(2), and that re-reduced in 5% H_2/Ar possessed a δ value of 0.040(2), which is exactly the same as the one for pristine $Sr_2MgMoO_{6-\delta}$ (sintered in 5% H_2/Ar).

Table 1
Oxygen nonstoichiometry parameter δ for the as-synthesized $Sr_2MMoO_{6-\delta}$ samples as determined by coulometric titration.

M	δ
Mg	0.040(2)
Mg, oxidized	0.000(2)
Mn	0.055(2)
Fe	0.041(7)
Co	−0.011(2)[a]
Ni	0.000(2)
Zn	0.000(2)

[a] Possibly due to a tiny impurity of Co_3O_4.

Rietveld refinement results for the as-synthesized samples are presented in Tables 2 and 3. First of all, we should mention that no indication of Mo-deficiency was found for any of the samples, even though $A_2B'MoO_6$ double-perovskite oxides have been suspected to be prone to Mo-deficiency due to the fact that MoO_3 has a relatively low melting temperature (ca. 795 °C) and might therefore volatilize during the high-temperature synthesis [34]. Fig. 5 shows the unit-cell volume of $Sr_2MMoO_{6-\delta}$ with M=Mg, Mn, Fe, Co, Ni and Zn as a function of ionic radius, $r(M^{2+})$ (assuming six-fold coordination and a high-spin state). It is seen that in the case of M=Mg, Zn and Ni the unit-cell volume increases linearly with increasing $r(M^{2+})$, while for M=Mn, Fe and Co, the cell volume is notably smaller than anticipated. Here it is interesting to recall the colors of the samples and to note that the

Table 2
Rietveld refinement results for the $Sr_2MMoO_{6-\delta}$ samples: lattice parameters and the values calculated for the Goldschmidt tolerance factor, t.

M	Mg	Mn	Fe	Co	Ni	Zn
Space group	I–1	I–1	I–1	I–1	I–1	I–1
a (Å)	5.5777(2)	5.6535(2)	5.57694(6)	5.5695(2)	5.55021(5)	5.5847(1)
b (Å)	5.5773(2)	5.6554(2)	5.57721(6)	5.5688(2)	5.55015(5)	5.5851(1)
c (Å)	7.92490(2)	8.0087(2)	7.90522(1)	7.95114(7)	7.89589(1)	7.97984(3)
α (deg)	89.897(2)	89.835(3)	89.960(1)	89.982(7)	89.978(1)	89.945(1)
β (deg)	90.117(2)	90.092(3)	90.0510(9)	89.959(3)	90.0392(9)	90.028(2)
γ (deg)	90.0846(5)	90.049(2)	90.0211(2)	89.998(4)	90.0114(5)	90.032(1)
V (Å^3)	246.528(9)	256.06(2)	245.882(4)	246.61(1)	243.229(3)	248.90(1)
R_{Bragg}	2.68	2.80	3.46	4.88	4.26	5.07
t	0.977	0.952	0.963	0.971	0.984	0.973

Table 3
Rietveld refinement results for the $Sr_2MMoO_{6-\delta}$ samples: atomic positions and occupancies and the values calculated for the degree of order parameter, S. Note that Mo is at site 2(a) (0, 0, 0) and M at site 2(b) (0.5, 0.5, 0.5).

M	Mg	Mn	Fe	Co	Ni	Zn
B overall	0.40(1)	0.66(1)	0.363(8)	0.09(2)	0.18(2)	0.51(1)
Sr						
x	0.4946(2)	0.4966(2)	0.5001(3)	0.5064(3)	0.4952(3)	0.5002(5)
y	−0.0012(4)	0.0032(3)	−0.0013(1)	−0.0003(8)	0.0003(6)	−0.0001(9)
z	0.2459(1)	0.2531(2)	0.2524(4)	0.2528(2)	0.2487(3)	0.2502(5)
Mo						
g_{Mo}	0.967	0.864	0.692	0.945	0.986	0.997
M						
g_M	0.967	0.864	0.692	0.945	0.986	0.997
S	0.933	0.728	0.384	0.890	0.972	0.994
O1						
x	−0.013(2)	0.068(1)	−0.009(1)	0.002(2)	−0.005(2)	0.0500(6)
y	−0.013(2)	0.017(2)	−0.001(1)	0.008(3)	−0.008(3)	0.009(2)
z	0.2372(3)	0.2380(8)	0.2420(2)	0.2413(3)	0.2419(3)	0.2349(4)
O2						
x	0.271(1)	0.263(1)	0.268(1)	0.201(1)	0.222(2)	0.249(2)
y	0.216(1)	0.194(1)	0.222(1)	0.300(1)	0.283(2)	0.224(2)
z	−0.014(1)	−0.019(1)	−0.0142(7)	−0.0342(6)	0.018(1)	0.0384(3)
O2b						
x	−0.215(2)	−0.203(1)	−0.220(1)	−0.256(1)	−0.255(2)	−0.207(2)
y	0.268(2)	0.260(2)	0.271(1)	0.213(1)	0.205(2)	0.276(2)
z	−0.0144(9)	0.012(2)	−0.0118(8)	−0.002(3)	0.010(2)	−0.001(3)

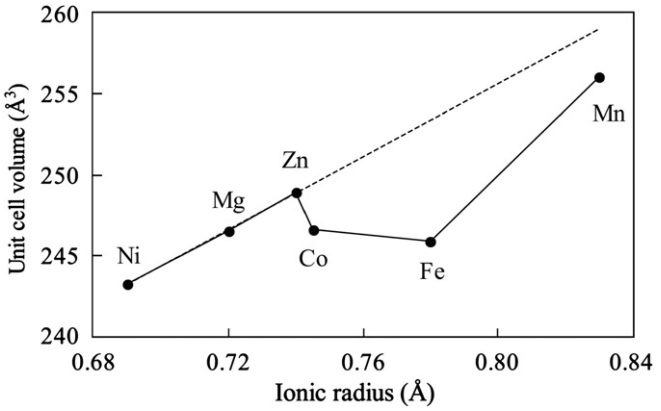

Fig. 5. Unit-cell volume plotted against the ionic radius of the *M* cation (assuming divalency) for the $Sr_2MMoO_{6-\delta}$ samples with *M*=Mg, Mn, Fe, Co, Ni and Zn. The dashed line is a guide to the eye.

samples with unit-cell volumes less than expected are all black, rather than non-black (which is the case for the other samples).

There are several possible explanations for the smaller-than-expected unit cell volumes of the *M*=Mn, Fe and Co samples. The most probable one is an *M*–Mo covalent charge transfer between the *B*-site cations. The sum of the valence numbers of the *B*-site cations in stoichiometric Sr_2MMoO_6 is +8, but this is satisfied by either the M^{II}/Mo^{VI} or the M^{III}/Mo^{V} state, or any mixture of the two. For all the three *M* constituents, Mn, Fe and Co, with the smaller-than-expected unit cell, the average size of the *B*-site cations is smaller for the M^{III}/Mo^{V} case than in the case of M^{II}/Mo^{VI}, and therefore the unit-cell volume will be smaller as well. We calculated the apparent M^{III}/M ratio from the refined unit-cell volumes by changing the amounts of M^{III}/Mo^{V} and M^{II}/Mo^{VI} until the calculated ionic radius matched the expected radius determined from the dashed line in Fig. 5. The calculations were done using the same ionic radii as in the calculation of the Goldschmidt tolerance factor earlier [31,32] and assuming linear dependency of the ionic radii between the M^{II}/Mo^{VI} and M^{III}/Mo^{V} states. We got the values of about 16% for Mn^{III}/Mn, 22% for Co^{III}/Co and 58% for Fe^{III}/Fe. In the latter case, the result is similar to the Fe^{III}/Fe ratio of 30–50% found by various other experimental methods and approaches (see the Introduction section) [19–21,37–39]. Actually, the electron transfer from the M^{II} valence state for *M*=Mn, Co and Fe is well-understood on the basis of reduction potentials. First of all, Mg and Zn are assumed to be divalent. The Ni^{III}/Ni^{II} reduction potential has been approximated to be relatively high, around 2.3 V [40], which would also favor the divalent state for Ni. The reduction potentials for Co^{III}/Co^{II}, Mn^{III}/Mn^{II} and Fe^{III}/Fe^{II} are 1.83, 1.54 and 0.77 V, respectively [30]. These lower reduction potentials could allow partial oxidation of the metals by a virtual electron transfer to Mo, and for Fe the redox energies may indeed overlap to give a real charge transfer.

It is also interesting to note that the degree of *B*-site order in the *M*=Mn, Fe and Co samples is somewhat lower than in the other samples (see Table 2). This could also be related to the possible mixed-valence state. The smaller charge difference between M^{III} and Mo^{V} compared to the difference between M^{II} and Mo^{VI} is expected to depress the ordering. However, the degree of order does not directly correlate with the determined M^{III}/M value: in case of *M*=Co, the degree of order is not as low as with *M*=Mn, even though their M^{III}/M values are roughly equal. This could be related to the fact that the *M*=Co sample was sintered at higher temperature, which is expected to favor higher ordering as long as it is controlled by the kinetics rather than thermodynamics [1,2].

Other phenomena, including a possible low spin state of the transition metal *M*, cation nonstoichiometry due to Mo deficiency, *B*-site cation disorder, and oxygen nonstoichiometry, may affect the unit-cell volume as well. However, the possibility for a low spin state for the M^{II} transition metals is negligible, and very large imbalances in cation stoichiometries would be needed to fully explain the smaller-than-expected unit cells. Cation disorder and oxygen vacancies are also expected to rather increase the unit-cell volume, not to decrease it. Therefore, these phenomena are not very likely to cause the smaller unit-cell volumes completely, but they may slightly affect the results.

4. Conclusions

The double-perovskites $Sr_2MMoO_{6-\delta}$ with *M*=Mg, Mn, Fe, Co, Ni, and Zn show different stabilities under reducing and oxidizing conditions. Consistent with a progressive lowering of the *M*-4*s* band energies and, from Fe to Zn, of the $M^{III/II}$ redox couples as the atomic number of the 3*d*-block cations increases, phases with *M*=Mn or Fe are stable under reducing conditions, but they become overoxidized to decompose in air. Moreover, these oxides show the strongest electron transfer from the M^{II} cations to Mo^{VI} with an apparent overlap of the $Fe^{III/II}$ and $Mo^{VI/V}$ redox energies. Phases with *M*=Co, Ni, or Zn, on the other hand, are stable under oxidizing conditions, but decompose in 5% H_2/Ar. The *M*=Mg phase, which has a higher energy 3*s* conduction band and no *d* electrons, was found to withstand both reductive and oxidative conditions with $\delta=0.04$ under 5% H_2/Ar and $\delta=0.00$ in air. All samples synthesized in air were oxygen stoichiometric; those synthesized in 5% H_2/Ar were oxygen-deficient.

Refined structural data were used to evaluate the degree of *B*-site order and to estimate, from comparison of experimental and predicted (on the basis of M^{II}-cation ionic radius) unit-cell volumes, the degree of real or virtual electron transfer from the M^{II} to the M^{VI} cations as a result of *M*–O–Mo interactions. Real electron transfer appears to occur for *M*=Fe as a result of an overlap of the $Fe^{III/II}$ and $Mo^{VI/V}$ redox energies. Consistent with the lowering of the $M^{III/II}$ redox energies with increasing atomic number, not only is the susceptibility to overoxidation reduced, but also the estimated electron transfer decreases progressively from *M*=Fe to Mn to Co to Ni, the $Mn^{III/II}$ being stabilized relative to the $Fe^{III/II}$ by the intra-atomic exchange stabilization of a high-spin $3d^5$ state.

Acknowledgment

The present work was supported by Academy of Finland (no. 126528) and Tekes (no. 1726/31/07).

References

[1] P. Woodward, R.-D. Hoffmann, A.W. Sleight, J. Mater. Res. 9 (1994) 2118.
[2] T. Shimada, J. Nakamura, T. Motohashi, H. Yamauchi, M. Karppinen, Chem. Mater. 15 (2003) 4494.
[3] Y.H. Huang, J. Lindén, H. Yamauchi, M. Karppinen, Chem. Mater. 16 (2004) 4337.
[4] F.K. Pattersson, C.W. Moeller, R. Ward, Inorg. Chem. 2 (1963) 196.
[5] F.S. Galasso, F.C. Douglas, R.J. Kasper, J. Chem. Phys. 44 (1966) 1672.
[6] T. Nakagawa, J. Phys. Soc. Jpn. 24 (1968) 806.
[7] K.-I. Kobayashi, T. Kimura, H. Sawada, K. Terakura, Y. Tokura, Nature 395 (1998) 677.
[8] M. Karppinen, H. Yamauchi, Chemistry of halfmetallic and related cation-ordered double perovskites, in: A.V. Narlikar (Ed.), Frontiers in Magnetic Materials, Springer Verlag, Berlin, 2005, pp. 153–184.
[9] Y.H. Huang, R.I. Dass, Z.L. Xing, J.B. Goodenough, Science 312 (2006) 254;
Y.H. Huang, R.I. Dass, J.C. Denyszyn, J.B. Goodenough, J. Electrochem. Soc. 153 (2006) A1266.

[10] Y. Matsuda, M. Karppinen, Y. Yamazaki, H. Yamauchi, J. Solid State Chem. 182 (2009) 1713.
[11] T. Yamamoto, J. Liimatainen, J. Lindén, M. Karppinen, H. Yamauchi, J. Mater. Chem. 10 (2000) 2342.
[12] Y. Yasukawa, J. Lindén, T.S. Chan, R.S. Liu, H. Yamauchi, M. Karppinen, J. Solid State Chem. 177 (2004) 2655.
[13] D.D. Sarma, P. Mahadevan, T. Saha-Dasgupta, S. Ray, A. Kumar, Phys. Rev. Lett. 85 (2000) 2549.
[14] Z. Fang, K. Terakura, J. Kanamori, Phys. Rev. B 63 (2001) 180407.
[15] H. Wu, Phys. Rev. B 64 (2001) 125–126.
[16] Z. Szotek, W.M. Temmerman, A. Svane, L. Petit, H. Winter, Phys. Rev. B 68 (2003) 104411.
[17] A.W. Sleight, J.F. Weiher, J. Phys. Chem. Solids 33 (1972) 679.
[18] J.B. Goodenough, R.I. Dass, Int. J. Inorg. Mater. 2 (2000) 3.
[19] J. Lindén, T. Yamamoto, M. Karppinen, H. Yamauchi, T. Pietari, Appl. Phys. Lett. 76 (2000) 2925.
[20] M. Karppinen, H. Yamauchi, Y. Yasukawa, J. Lindén, T.S. Chan, R.S. Liu, J.M. Chen, Chem. Mater. 15 (2003) 4118.
[21] Cz. Kapusta, P.C. Riedi, D. Zajac, M. Sikora, J.M. De Teresa, L. Morellon, M.R. Ibarra, J. Magn. Magn. Mater. 242–245 (2002) 701.
[22] B. García-Landa, C. Ritter, M.R. Ibarra, J. Blasco, P.A. Algarabel, R. Mahendiran, J. García, Solid State Commun. 110 (1999) 435.
[23] J.A. Alonso, M.T. Casais, M.J. Martínez-Lope, J.L. Martínez, P. Velasco, A. Munõz, M.T. Fernández-Díaz, Chem. Mater. 12 (2000) 161.
[24] Y. Moritomo, S. Xu, A. Machida, T. Akimoto, E. Nishibori, M. Takata, M. Sakata, K. Ohoyama, J. Phys. Soc. Jpn. 69 (2000) 1723.
[25] O. Chmaissem, R. Kruk, B. Dabrowski, D.E. Brown, X. Xiong, S. Kolesnik, J.D. Jorgensen, C.W. Kimball, Phys. Rev. B 62 (2000) 14197.
[26] M. Besse, V. Gros, A. Barthélémy, H. Jaffrès, J. Vogel, F. Petroff, A. Mirone, A. Tagliaferri, P. Bencok, P. Decorse, P. Berthet, Z. Szotek, W.M. Temmerman, S.S. Dhesi, N.B. Brookes, A. Rogalev, A. Fert, Europhys. Lett. 60 (2002) 608.
[27] J. Rodríguez-Carvajal, Physica B 192 (1993) 55–69.
[28] C. Bernuy-Lopez, M. Allix, C.A. Bridges, J.B. Claridge, M.J. Rosseinsky, Chem. Mater. 19 (2007) 1035.
[29] S. Vasala, M. Lehtimäki, S.C. Haw, J.M. Chen, R.S. Liu, H. Yamauchi, M. Karppinen, Solid State Ionics, submitted for publication.
[30] G. Milazzo, S. Carroli, Tables of Standard Electrode Potentials, John Wiley & Sons, New York, 1978.
[31] R.D. Shannon, Acta Crystallogr. A 32 (1976) 751.
[32] We calculated the t values assuming high-spin states for all the 3d cations and the following valence states and coordination numbers: Sr^{II} (CN=12), M^{II} (CN=6), Mo^{VI} (CN=6), O^{-II} (CN=6). r_B is an average of the ionic radii of the two B-site cations.
[33] Y.H. Huang, G. Liang, M. Croft, M. Lehtimäki, M. Karppinen, J.B. Goodenough, Chem. Mater. 21 (2009) 2319.
[34] D. Marrero-López, J. Penã-Martínez, J.C. Ruiz-Morales, D. Pérez-Coll, M.A.G. Aranda, P. Núñez, Mater. Res. Bull. 43 (2008) 2441.
[35] T. Wei, Y. Ji, X. Meng, Y. Zhang, Electrochem. Commun. 10 (2008) 1369.
[36] J.B. Goodenough, Y. Kim, J. Solid State Chem. 182 (2009) 2904.
[37] J. Navarro, J. Fontcuberta, M. Izquierdo, J. Avila, M.C. Asensio, Phys. Rev. B 70 (2004) 054423.
[38] K. Kuepper, I. Balasz, H. Hesse, A. Winiarski, K.C. Prince, M. Matteucci, D. Wett, R. Szargan, E. Burzo, M. Neumann, Phys. Stat. Sol. A 201 (2004) 3252.
[39] J. Rager, M. Zipperle, A. Sharma, J.L. MacManus-Driscoll, J. Am. Ceram. Soc. 87 (2004) 1330.
[40] S.G. Bratsch, J. Phys. Chem. Ref. Data 18 (1989) 1.